Manipulation and Characterization of Aqueous Sodium Dodecyl Sulfate/Sodium Chloride Aerosol Particles

Jariya Buajarern, Laura Mitchem, and Jonathan P. Reid*

School of Chemistry, University of Bristol, Bristol, BS8 1TS, United Kingdom

Received: August 9, 2007; In Final Form: October 7, 2007

Aerosol optical tweezers coupled with Raman spectroscopy can allow the detailed investigation of aerosol dynamics. We describe here measurements of the evolving size, composition, and phase of single aqueous aerosol droplets containing the surfactant sodium dodecyl sulfate and the inorganic salt sodium chloride. Not only can the evolving wet particle size be probed with nanometer accuracy, but we show that the transition to a metastable microgel particle can be followed, demonstrating that optical tweezers can be used to manipulate both spherical and non-spherical aerosol particles. Further, through the simultaneous manipulation and characterization of two aerosol droplets of different composition in two parallel optical traps, the phase behavior of a surfactant-doped particle and a surfactant-free droplet can be compared directly in situ. We also illustrate that the manipulation of two microgel particles can allow studies of the coagulation and interaction of two solid particles. Finally, we demonstrate that such parallel measurements can permit highly accurate comparative measurements of the evolving wet particle size of a surfactant-doped droplet with a surfactant-free droplet.

Introduction

Determining the phase and size of atmospheric particles at different relative humidities (RHs) is important for elucidating the role of particles in many atmospheric processes including the absorption and scattering of solar radiation, heterogeneous reactions between gas molecules and particles, and the activation of cloud condensation nuclei.[1−4] Hygroscopicity data are important for parametrizing thermodynamic models and interpreting the mixing state of atmospheric particles.[5−8] It is now widely recognized that understanding the impact of organic matter on the hygroscopicity of aerosol and the RH of phase transitions is of considerable importance. However, the influence of chemical composition on these properties remains poorly characterized and is not well-understood.[9] Unlike the inorganic fraction, which is now well-characterized, only a minor fraction of the organic components is even identified.[10,11]

Recent studies indicate that surface active organic components, or surfactants, can coat aerosol particles, leading to surface properties and chemical reactivities that are distinct from uncoated aerosols.[12−19] O'Dowd et al.[20] reported that marine aerosols contain significant concentrations of organic matter. Further, fatty acid salts and humic materials exist in marine aerosol in such sufficient quantities that they form micelle-like aggregates in solution.[21−24] Water-soluble organics form micelles when at concentrations greater than the critical micelle concentration (cmc), and water-insoluble organics can be solubilized within the micelles.[25] Further, the existence of organic films may impede the kinetics of hygroscopic growth of inorganic particles such as sodium chloride.[26,27] Studies have also shown that organic compounds can alter the hygroscopic properties of inorganic aerosol.[11,28,29] It has been shown that surfactants can reduce the hygroscopicity of the particle at high RHs but increase the hygroscopicity at low RHs. This is due to the formation of a liquid crystalline phase that can absorb a substantial amount of water at low RHs.[27,30]

In recent work, we have shown that the combination of optical tweezers and Raman spectroscopy can provide a valuable strategy for characterizing the properties and behavior of aerosol droplets. We have demonstrated that the unique capability of manipulating multiple aerosol particles in parallel optical traps can allow detailed measurements of aerosol interaction and coagulation[31,32] and can permit direct comparative measurements of the thermodynamic properties and kinetics of transformation of two aerosol particles of different composition.[33,34] Further, the properties of mixed-phase particles can be examined, and the formation of organic films on the surface of aqueous droplets characterized.[35,36]

We demonstrate here that a similar strategy can be adopted in the characterization of surfactant-doped aqueous droplets, allowing detailed measurements of composition, phase, and variation in wet particle size with variation in RH. In particular, we explore the properties of aqueous sodium chloride droplets containing the surfactant sodium dodecyl sulfate (SDS). Although SDS is not found in significant quantities in the atmosphere, its properties are often used to simulate the behavior of surfactants observed in the atmosphere.[30,37−40] The cmc of SDS decreases from 8.1 mM in pure water to 0.7 mM at a sodium chloride concentration of 300 mM.[41,42] Further, at such high concentrations of inorganic ions, charge shielding between micelles can lead to surfactant aggregation and the formation of a gel-like phase consisting of a porous network spanning the volume of a liquid medium.[42] Remaining mostly liquid in composition, such gels can exhibit densities similar to liquids with the structural coherence of a solid.

In the Experimental Procedures, we describe the experimental technique, before describing the spectroscopic characterization of mixed surfactant/sodium chloride droplets in Spectroscopy of Surfactant-Doped Aqueous Droplets. We then describe in Observing Phase Transitions in Surfactant/Inorganic/Aqueous Droplets the use of optical tweezers in studies of phase transformation and the ability to compare the phase behavior of two aerosol particles of different composition directly and

* Corresponding author. E-mail: j.p.reid@bristol.ac.uk.

10.1021/jp0764034 CCC: $37.00
Published on Web 11/29/2007

in situ by forming two optical traps. Finally, in Comparative Measurements of Equilibrium Wet Particle Sizes, we extend the comparative studies of two aerosol droplets to comparative measurements of the variation in wet particle size with variation in RH for two droplets, one doped with surfactant and the other surfactant-free.

Experimental Procedures

The aerosol optical tweezers instrument used in this work is similar in design to that described in previous work.[43] Light of wavelength 532 nm, generated by a Nd:YVO_4 laser (Coherent VERDI V5), is coupled into a polarization-maintaining single-mode fiber. The collimated output from the fiber passes through a half-wave plate and polarizing beam-splitter cube, permitting control over the power of the trapping laser beam. This also allows orthogonal linear polarizations of the laser light to be used to trap the particle. The beam passes through two sets of beam expansion optics, and the expanded laser beam is reflected off a narrow band mirror centered at 532 nm onto the back aperture of a 100× oil immersion objective (Olympic, NA 1.25). The particle is illuminated using focused light from a blue LED (centered at 455 nm, royal blue, Luxeon III Star, Lumileds). Two optical traps can be formed simultaneously using the approach developed by Fallman and Axner.[44] A beam splitter is inserted into the beam path at the conjugate plane of the back aperture of the microscope objective. This allows simultaneous control over two aerosol droplets, which can be separated by distances of up to 50 μm.[33]

The Raman backscatter from the trapped particle and the illumination light both pass through the narrow band mirror. The Raman light and blue illumination light are divided by a 50:50 beam splitter inclined at 45°. The transmitted Raman light is focused onto the entrance slit of a 0.5 m spectrograph (Spectra Pro 2500i Acton Research Corporation), dispersed by a diffraction grating (1200 g/mm), and collected with a CCD camera (Princeton Instruments). The Raman spectra are acquired with a spectral dispersion of 0.03 nm/pixel. Any unwanted elastic scatter from the laser is eliminated by an edge filter. Raman spectra are attained with 1 s time resolution. The blue light that is reflected off the beam splitter is projected onto a camera (Watec, 1/3 in. Color CCD Camera) after removing scattered laser light with a laser line filter, recording sequences of particle images with a time resolution of ~30 ms. This allows the acquisition of images from the underside of the droplet, referred to as in-plane imaging.

To capture images of the particle from the side in the horizontal plane, referred to as side imaging, windows are mounted on both sides of the cell. A white light source is used to illuminate the particle from one side of the cell. Images are acquired with the combination of 6.5× (UltraZoom, Navitar Machine Vision) and 20× (Mitoyu, NA 0.42, infinity corrected, Navitar Machine Vision) objective lenses from the other side of the cell. The overall magnification of the system is up to 45.72×, and the working distance is 25−30 mm.

Aqueous aerosol is generated using an Omron NE-U07 ultrasonic nebulizer. Typical solutions contain sodium chloride at a concentration of 0.20 M. The presence of the inorganic salt reduces the vapor pressure of the droplet, allowing the droplet to be retained indefinitely in the optical trap under subsaturated conditions.[45] The aqueous aerosol doped with SDS is also generated with an ultrasonic nebulizer. In most of the measurements presented here, an aqueous sodium chloride droplet is first loaded into the optical trap, and it is then bombarded with SDS-doped aqueous aerosols. Sodium chloride (>99%, analytical grade) was purchased from Fisher Scientific. SDS (>99.0% ACS reagent) was purchased from Sigma-Aldrich. All aqueous solutions were prepared in deionized water (HP 700 deionizer Purite).

Results and Discussion

We first consider the spectroscopic signature recorded from an optically tweezed surfactant-doped aqueous aerosol droplet before exploring the possibility of using optical tweezers to examine droplet-phase changes. In the final section, we describe a new experimental strategy for comparing directly and in situ the hygroscopic properties of two aerosol droplets of different chemical composition, specifically comparing the properties of a surfactant-doped aqueous sodium chloride droplet with a surfactant-free aqueous sodium chloride droplet.

Spectroscopy of Surfactant-Doped Aqueous Droplets. In previous work, we have demonstrated that Raman scattering from optically trapped aerosol droplets is consistent with that observed from a bulk sample. For example, we have established that the O−H Raman band shape shows an identical dependence on polarization and salt concentration in droplet and bulk-phase measurements.[46] Further, we have demonstrated that spectroscopic signatures of both organic and aqueous components can be observed in mixed-phase decane/water droplets.[32] In this study, we applied Raman spectroscopy to the determination of the composition of a trapped droplet that contains an involatile water-soluble organic.

In Figure 1a, we compare the spectra obtained from an aqueous sodium chloride droplet containing SDS at a concentration of 0.2 M and a bulk-phase sample of identical composition. In addition to the observation of spontaneous Raman scattering from the O−H stretching vibrations of water at Stoke's shifts greater than 3000 cm^{-1}, scattering from the C−H stretching vibrations of SDS was also observed at shifts below 3000 cm^{-1}. The continuous band envelopes from the spontaneous scattering are in excellent agreement, indicating that the droplet spectrum conforms to the bulk-phase measurement and that the composition of the droplet is equal to the bulk-phase solution from which it is generated. This conclusion is further reinforced from measurements of the refractive index of solutions prior to nebulization and the collected aerosol, which exhibit identical refractive indices with an absolute error of ±0.0001.[33]

It is also apparent from Figure 1a that the Raman scattering intensity is enhanced at wavelengths commensurate with whispering gallery modes (WGMs). At these discrete wavelengths, the Raman light can couple into the high-finesse cavity formed by the spherical droplet.[47,48] In previous publications, we have demonstrated that the size of a trapped droplet can be determined with nanometer accuracy from the unique fingerprint of WGM wavelengths appearing in the Raman fingerprint.[33,46] In the droplet spectrum shown in Figure 1a, the Raman scattering is enhanced by WGMs across the full breadth of the spectral fingerprint, over both the spontaneous O−H and the C−H stretching Raman bands. This suggests that both SDS and water molecules are probed within the volume explored by the WGMs, and this could be consistent with a homogeneous droplet of well-mixed organic and aqueous components or a core−shell droplet in which the organic component is concentrated within an outer shell.[36,46] We shall discuss this further in the next section.

Spontaneous Raman spectra recorded from bulk solutions of 0.2 M sodium chloride with SDS concentrations in the range of 0−0.2 M are illustrated in Figure 1b. The intensity of the C−H Raman band increases with the increase of the SDS

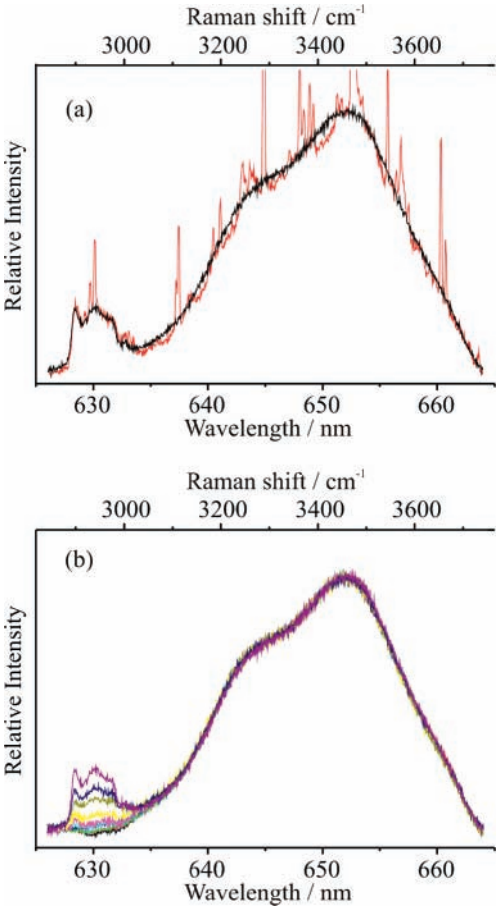

Figure 1. (a) Comparison of the Raman spectra observed from a trapped aqueous droplet (red) and a bulk-phase solution (black), both composed of 0.2 M SDS and 0.2 M sodium chloride. (b) Raman spectra of bulk-phase aqueous solutions of sodium chloride (0.2 M) with varying concentrations of SDS in the range of 0−0.2 M, illustrating the growth of the C−H stretching signature below a Raman shift of 3000 cm^{-1} with increasing concentration.

concentration. All spectra were corrected for background signals, eliminating any interference from Raman scattering generated by the microscope immersion oil, which also shows a signature in the C−H stretching region. It should be noted that the addition of SDS to the aqueous sodium chloride solution has no significant effect on the O−H Raman band shape, even at a SDS concentration of 0.2 M, a molar fraction of SDS of less than 0.005. Although the presence of sodium chloride has been observed to influence the shape of the O−H band at concentrations greater than 0.1 M,[46] the presence of the surfactant does not lead to a sufficient perturbation of the average hydrogen-bonding environment that it yields a spectroscopically distinct signature. It is likely that this is due to the dominant concentration of sodium chloride at all but the very highest surfactant concentrations presented here.

When determining the concentration of a dilute component within an aqueous aerosol, it is possible to use the signal intensity from the water component as an internal reference. Thus, by comparing the intensity of the C−H band with that of the O−H band, the droplet composition can be determined. In this study, we used Raman intensities at wavelengths of 628 and 652 nm (Stoke's shifts of 2870 and 3460 cm^{-1}, respectively) to determine the concentration of SDS relative to the concentration of water. These wavelengths correspond to the wavelengths of maximum intensity in the C−H and O−H Raman bands, respectively. Calibration curves for bulk-phase and single droplet

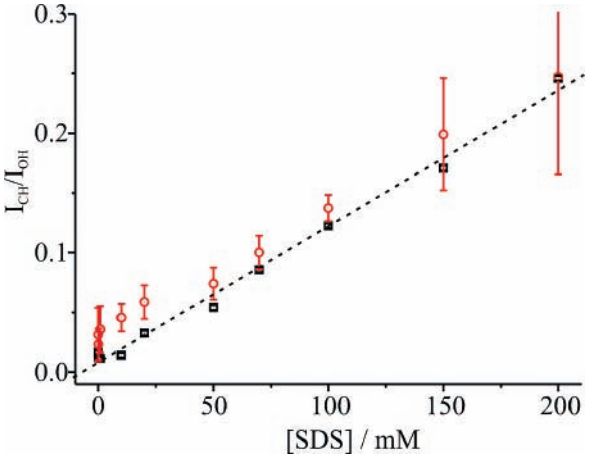

Figure 2. Calibration curves with varying SDS concentrations obtained from bulk-phase (black) and single droplet (red) measurements.

measurements were obtained and are illustrated in Figure 2. The error bars represent the standard deviation of the intensity ratio obtained from five different experiments. The calibration curves from the bulk-phase and single droplet measurements are in good agreement within the estimated errors. With decreasing SDS concentration, the droplet measurements are systematically higher in intensity ratio than those from bulk-phase measurements. This may be a consequence of the lower absolute signal intensities recorded from droplets than bulk samples and an increasing error in the subtraction of the contribution from the background immersion oil peak. Further, decreasing RH within the cell following aerosol capture leads to a decrease in the wet droplet size and an increase in the solute concentration. This could lead to droplet concentrations that are systematically higher than those used to record the bulk spectra. We will consider this in more detail in Comparative Measurements of Equilibrium Wet Particle Sizes. However, we can conclude here that the concentration can be determined with an error of ±10% at concentrations above 50 mM, with the error increasing significantly below 25 mM.

Observing Phase Transitions in Surfactant/Inorganic/Aqueous Droplets. We have demonstrated in previous work that aerosol optical tweezers can be used to investigate the controlled coagulation of aerosol droplets of different components.[32] This can allow studies of mixing state and phase behavior and could provide, for example, a strategy for controlling chemical transformations in picoliter volumes. We now examine the outcome of coagulation between two droplets, one containing only the surfactant SDS at high concentration (0.2 M) and the other containing only sodium chloride at high concentration (0.2 M). In the former droplet, the surfactant concentration is considerably higher than the cmc (8.1 mM).

The dependence of the aggregation number for SDS micelles on salt concentration has been well-characterized with the micelle size increasing with an increase in salt concentration.[42,49,50] In the absence of salt, the aggregation number at the cmc is reported to be ∼50, increasing to ∼120 at a sodium chloride concentration of ∼0.4 M with a surfactant concentration of 0.05 M. Further, a transition from a time averaged spherical micelle with an instantaneous flattened shape to a rod-like structure at high salt concentration has been reported.[51] Hayashi and Ikeda suggested that the formation of a metastable microgel could occur at high salt concentrations, formed from the aggregation of micelles and leading to the occlusion of water as the temperature of the solution is lowered and the solubility limit of SDS in the sodium chloride solution is approached.[42]

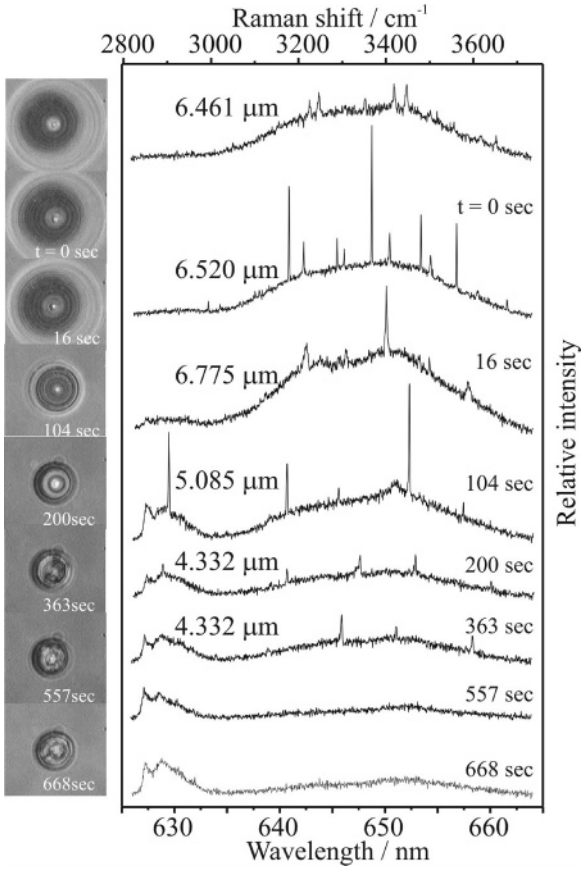

Figure 3. Sequence of evolving images and spectra from an aqueous sodium chloride droplet (0.2 M), dosed by coagulation with aqueous aerosol droplets of 0.2 M SDS. The first coagulation event occurs at $t = 0$ s.

It is expected that an aqueous droplet containing sodium chloride and SDS should form a supersaturated solution as water evaporates and the solubility limit of SDS is surpassed. At the elevated sodium chloride solutions present in the mixed droplet that result during evaporation, the micelles may aggregate, leading to the formation of a metastable microgel state with the possible eventual formation of small crystallites. In Figure 3, we report a typical example of the variation of the Raman spectrum and droplet image observed prior to and following a coagulation event. Initially, a homogeneous sodium chloride droplet is trapped and the spectrum recorded, allowing an accurate determination of the droplet size. Multiple coagulation events lead to an increase in droplet size by ~300 nm as the trapped sodium chloride aerosol droplet coagulates with droplets from an aqueous 0.2 M SDS aerosol flow. Sixteen seconds after the first coagulation event, the mixed component droplet begins to evaporate as the RH surrounding the droplet falls from close to saturation.[33] The loss in water leads to an increase in the C−H to O−H band intensity ratio, arising from an increase in the surfactant concentration.

Initially, the droplet appears homogeneous with the existence of micelles, which are expected to be less than 10 nm in size, not identifiable by brightfield microscopy or Raman spectroscopy. At 363 s following the first coagulation event, the droplet no longer appears homogeneous, and the formation of extended SDS agglomerates is apparent, either through the formation of a metastable microgel or through crystallization. The WGMs initially remain evident, indicating the presence of the residual aqueous phase at the droplet circumference. At times longer than 557 s after coagulation, the enhancement in the Raman signal is quenched as the WGMs are disrupted due to inhomogeneities in the refractive index,[32] leaving only the spontaneous Raman band. After this time, the droplet was observed to rotate in the trap with concerted rotation of the droplet inclusions. Further, the direction of rotation was found to depend on the polarization of the trapping beam.

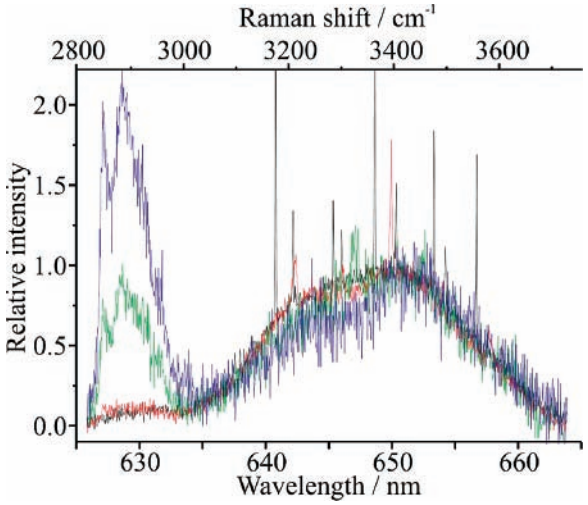

Figure 4. Comparison of the change in Raman spectra recorded during the evaporation of the multicomponent droplet formed by coagulation of an aqueous sodium chloride (0.2 M) droplet with aqueous aerosol containing SDS at a concentration of 0.2 M. The experiment is the same as that shown in Figure 3. Times: 0 s (black), 16 s (red), 200 s (green), and 668 s (blue) following coagulation.

The spontaneous Raman spectra of the aqueous SDS/sodium chloride droplet recorded at various times following coagulation are compared in Figure 4. The spectra are normalized by the maximum intensity of the O−H band, allowing comparison of the C−H band intensity and the O−H band shape. The observed increase in the spontaneous C−H band intensity relative to the O−H band of water confirms that the SDS concentration increases during the evaporation of the water component. Further, the spontaneous O−H band shape provides a signature of the hydrogen-bonding environment of the droplet bulk.[52−55] The shoulder at 3200 cm^{-1} decreases with time, indicating an increase of ionic strength due to an increase of the sodium chloride and SDS concentrations in the droplet and disruption of the hydrogen-bonding network. Notably, water is retained within the droplet during these measurements.

The evolving droplet radius was estimated from the change in WGM structure with time and by comparison with predictions from Mie calculations for scattering from a homogeneous spherical particle.[33,46] In all cases, the spectra are accurately modeled by the assumption of a uniform homogeneous refractive index, and no evidence for the formation of a core−shell structure or surface layers has been observed. The minimum detectable layer thickness in previous work has been 5 nm.[36] The refractive index formulation of Millard and Seaver[56] was used to determine the wavelength and concentration dependent refractive index of aqueous sodium chloride. The literature value of the refractive index increment for SDS, which defines the concentration dependence, was used to determine the refractive index of the solution.[57] The values calculated by this approach were compared with effective refractive index predictions, n_{eff}, determined using the Lorentz−Lorenz effective medium approximation,[58] and the values were the same within ±0.001. Assuming that this provides a measure of accuracy of the refractive index used for mixed component droplets, the error in the estimated droplet radius is <5 nm for droplets 5 μm in radius. The droplet size variation with time is indicated in Figure

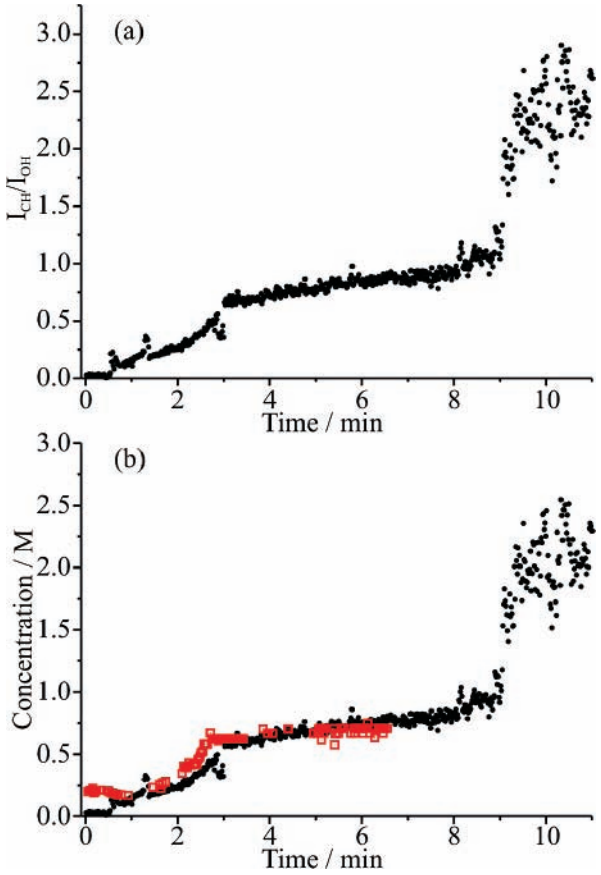

Figure 5. (a) Variation in the CH/OH Raman intensity ratio with time for the data set shown in Figure 3. (b) Estimated variations in the SDS concentration (black) and chloride ion concentration (red) with time. The SDS concentration was estimated using the bulk calibration curve presented in Figure 2. The chloride ion concentration was inferred from the variation of the droplet radius.

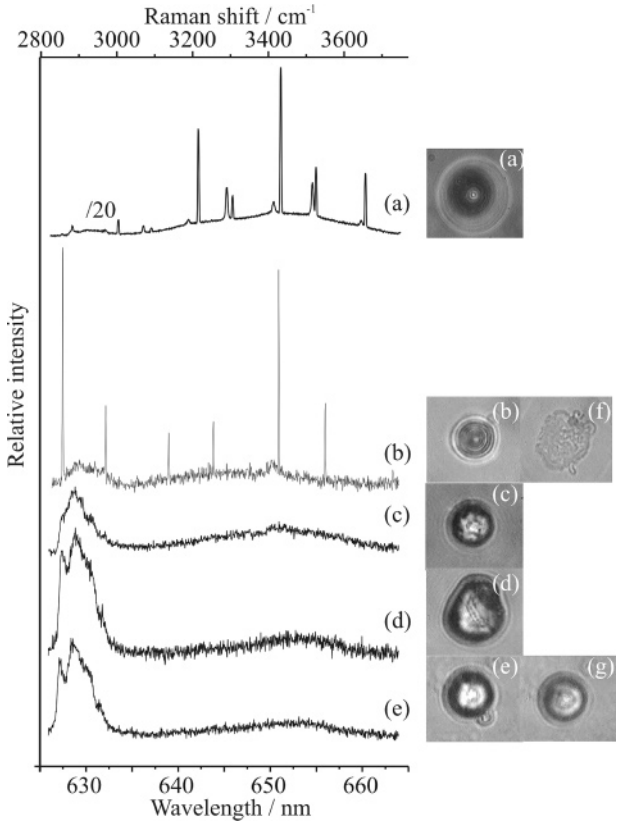

Figure 6. Comparison of the Raman spectra and images of aqueous sodium chloride/SDS droplets of varying composition and phase: (a) homogeneous liquid phase; (b) microgel phase with occluded water for which the WGMs were not quenched with (f) the resulting image once the particle is allowed to deposit on the coverslip; (c and d) further examples of the microgel phase; (e) a large microgel particle with a small particle attached to its surface, following which the smaller particle separates, as shown in panel g.

3, and all sizes should be assumed to have an associated accuracy of ±5 nm.

In principle, the evolving composition of the droplet can be determined from the variation in the intensity of the spontaneous Raman signature from the C−H vibrations (Figure 5a) or can be inferred from the variation in droplet size. The trapped droplet contains sodium chloride at a concentration of 0.2 M prior to coagulation with the SDS-doped aerosol. Given the sodium chloride concentration in the nebulized solution, the RH will be initially close to 99.35%.[59] On coagulation, the additional mass of solute leads to an increased mass loading of sodium ions in the droplet as well as introducing the organic component. Given the size change of the droplet from 6.461 to 6.775 μm, the organic component should be present only at concentrations of 0.03 M, with the sodium ion concentration remaining constant at 0.2 M and the chloride concentration dropping to 0.17 M. This ratio of chloride to SDS concentration should be retained throughout the experiment. These initial concentrations, estimated from the droplet size change, are consistent with the estimated concentration of SDS, determined from the C−H/O−H intensity ratio, reported in Figure 5b at times immediately after coagulation at 0 min.

After approximately 30 s, the C−H/O−H intensity ratio suggests a sudden increase in the surfactant concentration within the droplet. However, there is no comparable change in the droplet size. In previous work, we have noted that the trapping laser beam has a cross-section at focus that is geometrically smaller than the droplet and, thus, provides a spatially resolved signature of composition through the center of the droplet.[32] The sudden apparent increase in surfactant concentration without a corresponding change in size is thus likely to result from the formation of a surfactant-rich agglomerate that adopts a location centered within the trapping laser beam in the middle of the droplet.

At times longer than 7 min, the presence of substantially sized aggregates in the droplet, and the concomitant inhomogeneities in the refractive index, inhibits the observation of enhanced Raman scattering. Further, at times longer than ∼9 min, a significant fraction of the residual water is lost rapidly from the droplet as it forms a metastable microgel particle, although the Raman signature implies that there remains some occluded solvent. This leads to a sudden reduction in the signal intensity from water and, thus, considerable fluctuations in the intensity ratio as shown in Figure 5a. At this point, the particle has reached a SDS concentration of ∼0.8 M with a similar concentration of chloride. These conclusions are broadly consistent with the observations of Hayashi and Ikeda.[42] Solutions containing 0.6 and 0.8 M sodium chloride were found to be stable at 35 °C. However, lowering the temperature led to micelle association and the formation of a metastable microgel. Although SDS has a solubility limit of ∼0.9 M at 20 °C, the addition of sodium chloride leads to salting out of the organic component.[60]

Further experimental observations for aerosol particles doped with a range of surfactant mass fractions are reviewed in Figure 6. Each particle is formed from the coagulation of an aqueous

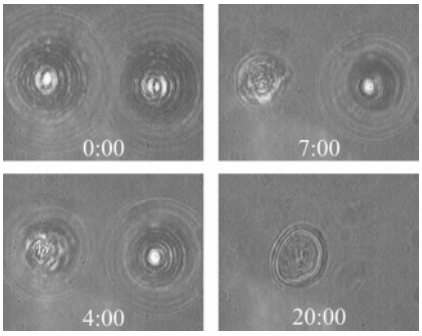

Figure 7. Direct comparison of the phase behavior with decreasing RH of an aqueous sodium chloride droplet (0.2 M) (right droplet) with an aqueous droplet containing SDS and sodium chloride at concentrations of 0.2 M (left droplet) at various times indicated in minutes. With decreasing wet particle size and increasing concentration, the SDS-doped droplets were observed to form a microgel particle after 7 min. At 20 min, both droplets were allowed to fall to the coverslip. While the residual surfactant is observed for the SDS-doped droplet, no residual material was left for the undoped droplet.

sodium chloride droplet of concentration 0.2 M with SDS droplets of varying concentrations. At initial SDS concentrations below 0.2 M, an aqueous SDS/sodium chloride droplet remains as a homogeneous liquid droplet with WGMs superimposed on both the O−H and the C−H stretching Raman bands (Figure 6a). At initial SDS concentrations higher than 0.2 M, a microgel phase forms (Figure 6(b−e). In all cases, the Raman signature of residual water suggests that it is present at high ionic strength. Mostly, the formation of aggregates leads to a quenching of the WGMs (Figure 6c), although on some occasions, the inhomogeneity in refractive index within the WGM probe volume is not sufficient to quench the WGMs entirely (Figure 6b). In this particular example, the presence of aggregate structures was confirmed by allowing the trapped particle to fall to the cover slip, allowing observation of the residual organic phase following the instantaneous loss of water (Figure 6f). In some instances, a composite particle can form that simultaneously possesses liquid and solid domains (Figure 6d). In many such examples, the composite particle is considerably deformed from sphericity. Indeed, Figure 6e,g suggests that under some circumstances, particle separation can occur with, in this case, the loss of a small fragment particle from the edge of a large particle. Importantly, it should be noted that these studies provide the first evidence that solid non-spherical particles can be manipulated with aerosol optical tweezers.

We now demonstrate that it is possible to compare directly in situ the phase behavior of a surfactant-doped sodium chloride droplet with a surfactant-free sodium chloride droplet. As described in the Experimental Procedures, two optical traps can be readily formed, allowing the simultaneous manipulation of two particles and the direct comparison of particles of different composition. Figure 7 illustrates this approach, representing the first opportunity to directly compare a surfactant-doped droplet and a surfactant-free droplet simultaneously within the same environment. A surfactant-doped aqueous sodium chloride droplet is first loaded into the left-hand optical trap. This is followed by the capture of an aqueous sodium chloride droplet in the second optical trap. In these measurements, no accurate measurements of the evolving RH near the two droplets were possible,[46] although the RH decreases with time following the initial nebulization/trapping step. Although both droplets are initially observed to be liquid, the formation of aggregates in the surfactant-doped droplet is apparent after 4 min. Allowing the two aerosol particles to settle to the coverslip after 20 min

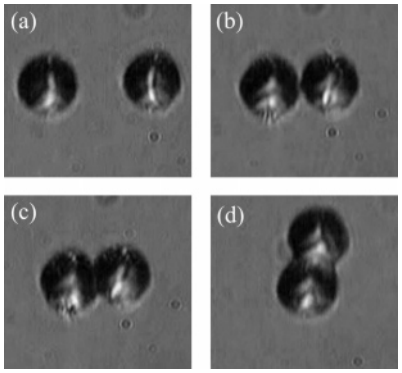

Figure 8. Example of controlled coagulation of two SDS/sodium chloride microgel particles. The images were captured using side imaging: (a) two individual microgel particles; (b) gel particles just prior to coagulation; (c) at coagulation; and (d) after coagulation with the translation of the left trap away from the composite particle.

confirms the formation of a microgel in the organic-doped droplet with a loss of residual water. Given that the efflorescence RH for aqueous sodium chloride droplets is ∼45%,[61] the metastable microgel organic phase must be formed at a higher RH at which the aqueous sodium chloride droplet remains in liquid form. Clearly, such direct comparative measurements of the behavior of two aerosol particles provide a valuable new strategy for examining the behavior of two particles of differing composition.

In a further application of the ability to manipulate solid aerosol particles, we illustrate in Figure 8 that two solid SDS microgel particles can be simultaneously manipulated leading to controlled coalescence. In this example, images are recorded from the side, as described in the Experimental Procedures. Images of the two particles prior to, during, and after coagulation are illustrated. Two aqueous SDS/sodium chloride droplets were trapped and left to evaporate until they transformed to the metastable microgel phase. Unlike previous examples given by us of the controlled coagulation of liquid droplets, the particles adhere, forming a composite conjoined particle as shown in Figure 8c. On separation of the two optical traps, the particles remain conjoined and retained in one of the optical traps.

Comparative Measurements of Equilibrium Wet Particle Sizes. We now examine directly the variation in wet particle size of two droplets in parallel, one doped with surfactant and one without. In this section, we explore the influence of SDS on the equilibrium size of an aqueous sodium chloride droplet at low surfactant mass fraction. In previous work, we have demonstrated that although the wet particle size variation with RH can be measured accurately for a single particle with the aerosol optical tweezers approach, the largest uncertainty in the measurement arises in the determination of the RH.[46] The capacitance probe used in these previous measurements had a slow time response (50 s) and was inaccurate at RHs over 90%, with an accuracy at lower RHs of ±2%. Further, the initial flow of wet aerosol into the cell gave rise to significant spatial variations in RH: the RH measured by the RH probe at the top of the aerosol cell was found to be different from the RH experienced by the trapped droplet sitting a few tens of microns above the glass coverslip. In more recent work, we have demonstrated that the wet particle size of a control sodium chloride droplet can be used to determine the RH with an absolute accuracy of better than 0.1% at all RHs, even at RHs approaching saturation.[33] Thus, a droplet of known composition can provide an extremely accurate probe of RH with high spatial and temporal resolution. In this section, we exploit a control

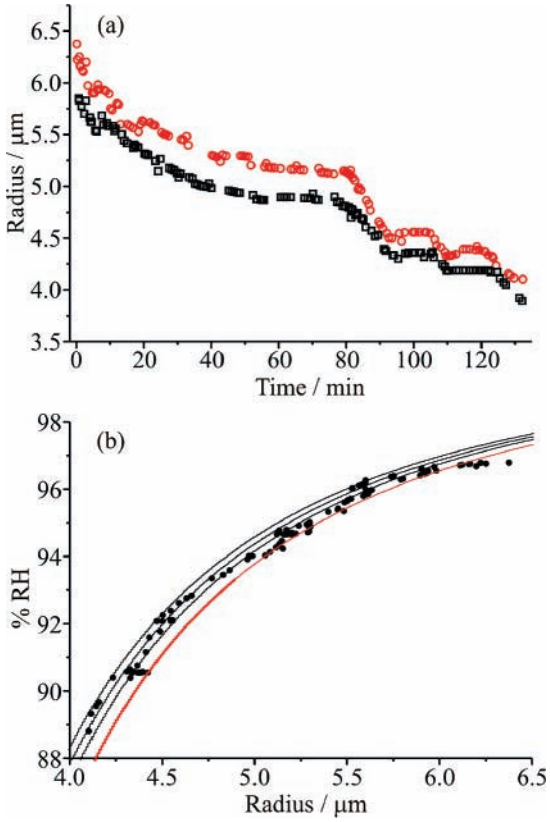

Figure 9. (a) Simultaneous measurements of the time dependence of the size of two droplets. An aqueous droplet containing SDS at a concentration of 10 mM and sodium chloride at 0.85 M (red circles) is compared with an aqueous droplet containing only the sodium chloride component (0.85 M, black squares). (b) Comparison of the experimentally measured Köhler curve for the surfactant-doped droplet (filled circles) with calculated Köhler curves for aqueous sodium chloride droplets with dry particle radii of 1740, 1760, 1780 (black lines from top to bottom), and 1814 nm (red).

aqueous sodium chloride droplet, trapped alongside a droplet containing the surfactant, to determine the RH accurately and with a high time resolution. The impact of the surfactant on the hygroscopicity of a sodium chloride droplet can then be investigated directly.

An aqueous sodium chloride droplet (0.85 M), the control droplet, and an aqueous sodium chloride droplet (0.85 M) doped with 10 mM SDS, the surfactant-doped droplet, were trapped in two optical traps and held at a separation of ~30 μm. Both droplets were assumed to contain the same sodium chloride concentration as the nebulized solution. The surface area occupied by a SDS molecule at an aqueous sodium chloride surface can be assumed to be ~36 Å^2.[62] The SDS concentration required to accomplish complete coverage of the droplet surface increases with a decrease in droplet radius due to the increasing surface/volume ratio. Complete surface coverage can be achieved at a SDS concentration of ~2 mM for a 6 μm radius droplet. It should be noted that the cmc of SDS in a 0.2 M sodium chloride aqueous solution is ~1 mM.[63−65] Therefore, at SDS concentrations above 1 mM, the micellization of SDS molecules is expected to occur as well as the formation of a monomolecular film.

Figure 9a illustrates the variation in the two droplet radii over time as the RH in the cell drops and the wet particle size decreases. The refractive indices for both droplets were assumed to be determined by the concentration of the sodium chloride component, following the procedure described in Observing Phase Transitions in Surfactant/Inorganic/Aqueous Droplets. On the basis of the determination of the initial wet particle size and, thus, the mass loading of sodium chloride in the control droplet, the equivalent dry particle size of 1664 nm (41.8 pg) can be estimated from the density of sodium chloride (2.17 g cm^{-3}). An associated error of 0.5% in the dry particle mass can be assumed.[33] Hence, the Köhler curve of a pure sodium chloride particle of dry radius of 1664 nm was obtained using the AIM model.[33,59] From the theoretical variation in wet particle size with RH, the variation in the wet size of the control droplet with time was used to determine the variation in local RH with time. On the basis of our previous analysis, all RHs can be assumed to have an associated accuracy of ±0.09%.[33] Once the time variation in RH is known, the experimental Köhler curve of the surfactant-doped droplet can be viewed directly, as shown in Figure 9b.

Along with the experimentally determined Köhler curve shown in Figure 9b, curves calculated for pure sodium chloride particles of dry radii 1740, 1760, 1780, and 1814 nm are shown for comparison. The initial experimental wet droplet size can be used to estimate the mass loading of sodium chloride in the surfactant-doped droplet, and this is equivalent to a dry sodium chloride particle of 1814 nm radius. It is clear from the comparison that the agreement between the measurements and predictions is excellent, particularly at early time and high RH. As the droplet evaporates to a smaller size, the droplet deviates increasingly from the predicted Köhler curve. However, Sorjamaa et al.[66] have demonstrated that including the surfactant explicitly in the Köhler analysis, through its influence on the surface tension and the Raoult effect, increases the RH at which a particular wet droplet size is at equilibrium, in line with the measurements presented here. The influence of the surfactant diminishes at high RHs with an increase in wet particle size and decrease in concentration. We have not included a comparison between our measurements and this treatment here as the assumption must be made that the solution is dilute.[66] Given the accuracy of our measurements, this does not provide a sufficiently verifiable comparison for only one experimental data set. Thus, a fuller analysis is beyond the scope of the current work but will be explored in a future publication.

In the discussion of Figure 9, we have assumed that both droplets always exist in an equilibrium state with the surrounding gas phase on the time scale of 1 s, the time resolution of the size measurements. Clearly, an important future development with this measurement strategy will be to explore the possible kinetic limitations imposed on droplet size changes through the presence of a surface active organic component. It has been suggested that not only can the presence of organic components influence the thermodynamic properties of aerosols, but they can also influence the rate of mass transfer.[30,39,67,68] On the time scale of these measurements, there is no apparent difference in the time response of the size of surfactant-doped and -free droplets, consistent with the expected behavior of droplets with a low mass fraction of the organic component and the Knudsen number of the droplets held in a gas phase at atmospheric pressure.

Conclusion

We demonstrate that the equilibrium size and phase of a sodium chloride/surfactant particle with varying RH can be investigated by coupling aerosol optical tweezers with Raman spectroscopy. The Raman signature can allow the determination of the concentration of the surfactant and can allow interrogation of the hydrogen-bonding network of the aqueous component. Variations in size, composition, and phase can be investigated

with 1 s time resolution. At high SDS and sodium chloride concentrations, SDS is observed to form a metastable microgel, consistent with observations in bulk-phase measurements. Further, we demonstrate that comparative measurements of phase behavior can be made, comparing directly and in situ the phase behavior of two aerosol droplets, one containing surfactant and one not. This is the first demonstration of the application of optical tweezers to studies of non-spherical solid particles. This approach differs from optical levitation measurements, in which radiation pressure balances gravity, by using the optical gradient force to not only trap the particle but to manipulate it. Notably, this has led to the first observation of the controlled coalescence of two solid particles.

In a final measurement, we demonstrate that a dual optical trap approach can provide a method to accurately investigate and compare the properties of a surfactant-doped droplet with a control surfactant-free droplet. Direct comparative measurements have been performed, allowing an examination of the effect of SDS on the hygroscopicity of a sodium chloride droplet. A control sodium chloride droplet has been used as a RH probe for the accurate determination of gas-phase composition locally at high RHs (>90%). Further, it is anticipated that such a strategy may allow detailed measurements of the kinetics of mass transfer, permitting a direct study of the influence of surface active organic films on the rate of uptake of water and other trace species.

In summary, we have demonstrated that aerosol optical tweezers can provide a versatile strategy for characterizing and comparing the thermodynamic properties of aerosol particles. This can extend to the characterization of phase transitions and studies of aerosol coagulation and interaction. Future measurements will seek to explore the kinetic limitations imposed on mass transfer by organic films.

Acknowledgment. We acknowledge the EPSRC for financial support and for supporting L.M. during the early stages of this work. Support from NERC through the APPRAISE program is also acknowledged. The Royal Thai government is acknowledged for studentship support for J.B.

References and Notes

(1) Martin, S. T.; Hung, H. M.; Park, R. J.; Jacob, D. J.; Spurr, R. J. D.; Chance, K. V.; Chin, M. *Atmos. Chem. Phys.* **2004**, *4*, 183.
(2) Tang, I. N.; Munkelwitz, H. R. *J. Appl. Meteorol.* **1994**, *33*, 791.
(3) Hu, J. H.; Abbatt, J. P. D. *J. Phys. Chem. A* **1997**, *101*, 871.
(4) Chan, M. N.; Chan, C. K. *Atmos. Chem. Phys.* **2005**, *5*, 2703.
(5) Cocker, D. R.; Whitlock, N. E.; Flagan, R. C.; Seinfeld, J. H. *Aerosol Sci. Technol.* **2001**, *35*, 637.
(6) Topping, D. O.; McFiggans, G. B.; Coe, H. *Atmos. Chem. Phys.* **2005**, *5*, 1205.
(7) Topping, D. O.; McFiggans, G. B.; Coe, H. *Atmos. Chem. Phys.* **2005**, *5*, 1223.
(8) Clegg, S. L.; Brimblecombe, P.; Liang, Z.; Chan, C. K. *Aerosol Sci. Technol.* **1997**, *27*, 345.
(9) Marcolli, C.; Luo, B. P.; Peter, T. *J. Phys. Chem. A* **2004**, *108*, 2216.
(10) Chan, M. N.; Choi, M. Y.; Ng, N. L.; Chan, C. K. *Environ. Sci. Technol.* **2005**, *39*, 1555.
(11) Peng, C.; Chan, M. N.; Chan, C. K. *Environ. Sci. Technol.* **2001**, *35*, 4495.
(12) Hameri, K.; Rood, M.; Hansson, H.-C. *J. Aerosol Sci.* **1992**, *23*, 437.
(13) Law, N. L.; Diamond, M. L. *Chemosphere* **1998**, *36*, 2607.
(14) Donaldson, D. J.; Vaida, V. *Chem. Rev.* **2006**, *106*, 1445.
(15) Eliason, T. L.; Gilman, J. B.; Vaida, V. *Atmos. Environ.* **2004**, *38*, 1367.
(16) Seidl, W. *Atmos. Environ.* **2000**, *34*, 4917.
(17) Jacobson, M. Z. *Nature (London, U.K.)* **2001**, *409*, 695.
(18) Menon, S.; Hansen, J.; Nazarenko, L.; Luo, Y. *Science (Washington, DC, U.S.)* **2002**, *297*, 2250.
(19) Daumer, B.; Niessner, R.; Klockow, D. *J. Aerosol Sci.* **1992**, *23*, 315.
(20) O'Dowd, C. D.; Facchini, M. C.; Cavalli, F.; Cebrunis, D.; Mircea, M.; Decesari, S.; Fuzzi, S.; Yoon, Y. J.; Putaud, J.-P. *Nature (London, U.K.)* **2004**, *431*, 676.
(21) Kokkola, H.; Sorjamaa, R.; Peraniemi, A.; Raatikainen, T.; Laaksonen, A. *Geophys. Res. Lett.* **2006**, *33*, 10816.
(22) Krivacsy, Z.; Kiss, G.; Varga, B.; Galambos, I.; Sarvari, Z.; Gelencser, A.; Molnar, A.; Fuzzi, S.; Facchini, M. C.; Zappoli, S.; Andracchio, A.; Alsberg, T.; Hansson, H. C.; Persson, L. *Atmos. Environ.* **2000**, *34*, 4273.
(23) Graber, E. R.; Rudich, Y. *Atmos. Chem. Phys.* **2006**, *6*, 729.
(24) Kiss, G.; Tombacz, E.; Hansson, H.-C. *J. Atmos. Chem.* **2005**, *50*, 279.
(25) Tabazadeh, A. *Atmos. Environ.* **2005**, *39*, 5472.
(26) Hansson, H. C.; Rood, M. J.; Koloutsou-Vakakis, S.; Hameri, K.; Orsini, D.; Wiedensohler, A. *J. Atmos. Chem.* **1998**, *31*, 321.
(27) Andreas, E. L. *J. Geophys. Res.* **1992**, *97*, 11429.
(28) Rissler, J.; Swietlicki, E.; Zhou, J.; Roberts, G. C.; Andreae, M. O.; Gatti, L. V.; Artaxo, P. *Atmos. Chem. Phys.* **2004**, *4*, 2119.
(29) Kredenweis, S. M.; Koehler, K.; DeMott, P. J.; Prenni, A. J.; Carrico, C.; Ervens, B. *Atmos. Chem. Phys.* **2005**, *5*, 1357.
(30) Chen, Y.-Y.; Lee, W.-M. G. *Chemosphere* **1999**, *38*, 2431.
(31) Buajarern, J.; Mitchem, L.; Ward, A. D.; Nahler, N. H.; McGloin, D.; Reid, J. P. *J. Chem. Phys.* **2006**, *125*, 114506.
(32) Mitchem, L.; Buajarern, J.; Ward, A. D.; Reid, J. P. *J. Phys. Chem. B* **2006**, *110*, 13700.
(33) Butler, J. R.; Mitchem, L.; Hanford, K. L.; Treuel, L.; Reid, J. P. *Faraday Discuss.* **2007**, in press.
(34) Mitchem, L.; Hopkins, R. J.; Buajarern, J.; Ward, A. D.; Reid, J. P. *Chem. Phys. Lett.* **2006**, *432*, 362.
(35) Buajarern, J.; Mitchem, L.; Reid, J. P. *J. Phys. Chem. A* **2007**, in press.
(36) Buajarern, J.; Mitchem, L.; Reid, J. P. *J. Phys. Chem. A* **2007**, submitted.
(37) Snead, C. C.; Zung, J. T. *J. Colloid Interface Sci.* **1968**, *27*, 25.
(38) Lo, J.-H. A.; Lee, W.-M. G. *Chemosphere* **1996**, *33*, 1391.
(39) Shulman, M. L.; Charlson, R. J.; Davis, E. J. *J. Aerosol Sci.* **1997**, *28*, 737.
(40) Li, Z.; Williams, A. L.; Rood, M. J. *J. Atmos. Sci.* **1998**, *55*, 1859.
(41) Chen, J.-M.; Su, T.-M.; Mou, C. Y. *J. Phys. Chem.* **1986**, *90*, 2418.
(42) Hayashi, S.; Ikeda, S. *J. Phys. Chem.* **1980**, *84*, 744.
(43) Knox, K. J.; Reid, J. P.; Handford, K. L.; Hudson, A. J.; Mitchem, L. *J. Opt. A: Pure Appl. Opt.* **2007**, *9*, 180.
(44) Fallman, E. F.; Axner, O. *Appl. Opt.* **1997**, *36*, 2107.
(45) Hopkins, R. J.; Mitchem, L.; Ward, A. D.; Reid, J. P. *Phys. Chem. Chem. Phys.* **2004**, *6*, 4924.
(46) Mitchem, L.; Buajarern, J.; Hopkins, R.; Ward, A. D.; Gilham, R. J. J.; Johnson, R. L.; Reid, J. P. *J. Phys. Chem. A* **2006**, *110*, 8116.
(47) Hill, S. C.; Benner, R. E. *J. Opt. Soc. Am. B* **1986**, *3*, 1509.
(48) Hill, S. C.; Rushforth, C. K.; Benner, R. E.; Conwell, P. R. *Appl. Opt.* **1985**, *24*, 2380.
(49) Quina, F. H.; Nassar, P. M.; Bonilha, J. B. S.; Bales, B. L. *J. Phys. Chem.* **1995**, *99*, 17028.
(50) Rharbi, Y.; Chen, L.; Winnik, M. A. *J. Am. Chem. Soc.* **2004**, *126*, 6025.
(51) Cabane, B.; Duplessix, R.; Zemb, T. *J. Phys.* **1985**, *46*, 2161.
(52) Starzak, M.; Mathlouthi, M. *Food Chem.* **2003**, *82*, 3.
(53) Sceats, M. G.; Stavola, M.; Rice, S. A. *J. Chem. Phys.* **1979**, *70*, 3927.
(54) Carey, D. M.; Korenowski, G. M. *J. Chem. Phys.* **1998**, *108*, 2669.
(55) Li, R.; Jiang, Z.; Chen, F.; Yang, H.; Guan, Y. *J. Mol. Struct.* **2004**, *707*, 83.
(56) Millard, R. C.; Seaver, G. *Deep-Sea Res.* **1990**, *37*, 1909.
(57) Mysels, K. J.; Princen, L. H. *J. Phys. Chem.* **1959**, *63*, 1696.
(58) Chen, J.-P.; Chao, S.; Kao, J.-S.; Niu, H.; Chen, C.-H. *Appl. Opt.* **1996**, *35*, 90.
(59) Clegg, S. L.; Wexler, A. S. On-line Aerosol Inorganics Model.
(60) Bales, B. L.; Messina, L.; Vidal, A.; Peric, M. *J. Phys. Chem. B* **1998**, *102*, 10347.
(61) Hamilton, J. F.; Lewis, A. C.; Reynolds, J. C.; Carpenter, L. J.; Lubben, A. *Atmos. Chem. Phys.* **2006**, *6*, 4973.
(62) Johnson, C. M.; Tyrode, E. *Phys. Chem. Chem. Phys.* **2005**, *7*, 2635.
(63) Besio, G. J.; Prud'homme, R. K.; Benziger, J. B. *Langmuir* **1988**, *4*, 140.
(64) Almgren, M.; Swarup, S. *J. Colloid Interface Sci.* **1983**, *9*, 256.
(65) Varela, A. S.; Macho, M. I. S.; Gonzalez, A. G. *Colloid Polym. Sci.* **1995**, *273*, 876.
(66) Sorjamaa, R.; Svenningsson, B.; Raatikainen, T.; Henning, S.; Bilde, M.; Laaksonen, A. *Atmos. Chem. Phys.* **2004**, *4*, 2107.
(67) Smoydzin, L.; Glasow, R. *Atmos. Chem. Phys. Discuss.* **2006**, *6*, 10373.
(68) Rudich, Y. *Chem. Rev.* **2003**, *103*, 5097.